CHAPTER IV

RESULTS AND DISCUSSION

In this chapter, the synthesis and characterization of catalysts were described. The oxidation of model sulfur compounds (benzothiophene, dibenzothiophene and 4,6-dimethyldibenzothiophene) with hydrogen peroxide catalyzed by these synthesized catalysts were studied. Finally, the catalytic system was utilized in the oxidation of diesel fuels.

4.1 Synthesis of catalysts

The synthesized catalysts are listed below:

Disodium acidic salts:	$Na_2H[PMo_{12}O_{40}]$	$Na_2H[PW_{12}O_{40}]$
Acids:	$H_3PMo_{12}O_{40}$	$H_3PW_{12}O_{40}$
Vanadyl acidic salts:	$(VO)H[PMo_{12}O_{40}]$	$(VO)H[PW_{12}O_{40}]$

Tetrabutylammonium salts of tungstophosphate:

$(n\text{-}Bu_4N)_3[PW_{12}O_{40}]$

Tetrabutylammonium salts of tungsto vanadophosphate:

$(n\text{-}Bu_4N)_4[PVW_{11}O_{40}]$

$(n\text{-}Bu_4N)_5[PV_2W_{10}O_{40}]$

$(n\text{-}Bu_4N)_6[PV_3W_9O_{40}]$

Disodium acidic salts:

$Na_2MoO_4.2H_2O$ or $Na_2WO_4.2H_2O + H_2O + 85\%H_3PO_4 + 70\%HClO_4$

↓

Greenish crystals for $Na_2H[PMo_{12}O_{40}]$ or white crystals for $Na_2H[PW_{12}O_{40}]$

Acids:

$Na_2H[PMo_{12}O_{40}]$ or $Na_2H[PW_{12}O_{40}]$ + H_2O + HCl

↓

Yellow crystal for $H_3PMo_{12}O_{40}$ or white crystal for $H_3PW_{12}O_{40}$

Vanadyl acidic salts:

$H_3PMo_{12}O_{40}$ or $H_3PW_{12}O_{40}$ + $C_{10}H_{14}VO_5$ in toluene

↓

Light green crystals for $(VO)H[PMo_{12}O_{40}]$ or dark green crystal for $(VO)H[PW_{12}O_{40}]$

Tetrabutylammonium salts of tungstophosphate:

$Na_2WO_4.2H_2O$ + H_2O + 85%H_3PO_4 + H_2SO_4

↓ *n*-Bu_4NBr

White crystals for $(n\text{-}Bu_4N)_3[PW_{12}O_{40}]$

Tetrabutylammonium salts of tungsto vanadophosphate:

$NaH_2PO_4.2H_2O$ + $Na_2WO_4.2H_2O$ + H_2O

↓ Stock solution: NH_4VO_3 + NaOH + H_2O

5 mL	20 mL	80 mL
↓	↓	↓
Yellow solution	Orange solution	Dark orange solution
↓ *n*-Bu_4NBr	↓ *n*-Bu_4NBr	↓ *n*-Bu_4NBr
Yellow crystals for $(n\text{-}Bu_4N)_4[PVW_{11}O_{40}]$	Orange crystals for $(n\text{-}Bu_4N)_5[PV_2W_{10}O_{40}]$	Dark orange crystals for $(n\text{-}Bu_4N)_6[PV_3W_9O_{40}]$

The synthesized catalysts were characterized. The property of catalysts were described and discussed as follows:

4.2 Characterization of catalysts

4.2.1 Phase analysis of catalysts

The phase analysis of the synthesized polyoxometalate catalysts are characterized by XRD technique. The XRD pattern of polyoxometalate catalysts presented the typical pattern of heteropoly compound. The XRD pattern of synthesized $H_3PW_{12}O_{40}$ compared with the pattern from Yang *et al.* [24] are shown in Figure 4.1.

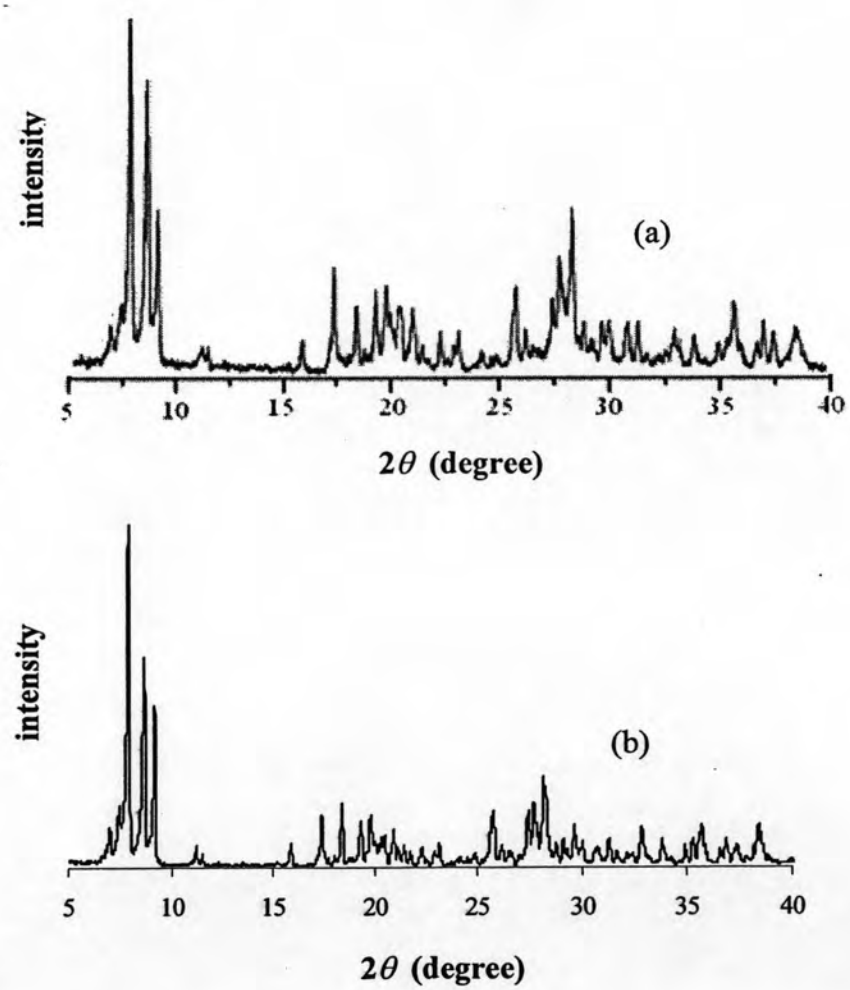

Figure 4.1 XRD patterns of
(a) $H_3PW_{12}O_{40}$ from Yang *et al.* [24].
(b) $H_3PW_{12}O_{40}$ from this work.

It can be seen that the diffraction peaks in the XRD pattern of the synthesized $H_3PW_{12}O_{40}$ (Figure 4.1b), were observed at 2θ, degree (lattice plane) = 7.1 (001), 8.0 (110), 8.8 (011), 9.2 (101) and 18.5 (202). The XRD pattern was similar to that previously reported by Yang *et al.* [24] and [JCPDF 50-0656].

The XRD pattern of the molybdenum containing catalyst, $H_3PMo_{12}O_{40}$ is shown in Figure 4.2.

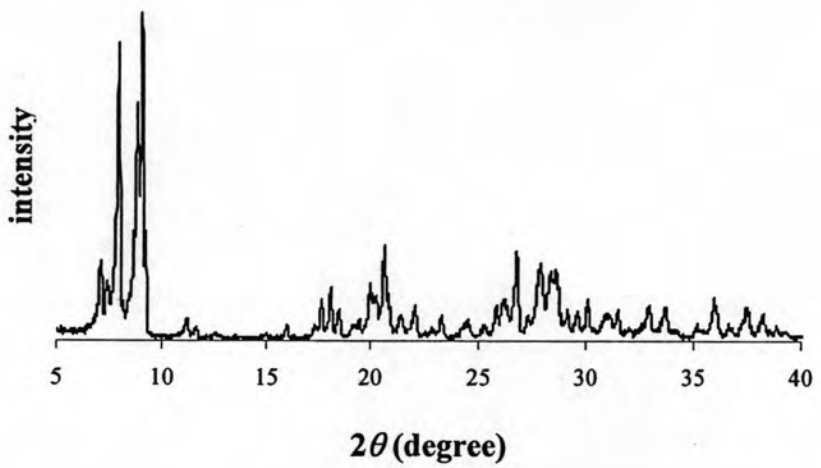

Figure 4.2 XRD pattern of $H_3PMo_{12}O_{40}$.

From Figure 4.2, the diffraction peaks of $H_3PMo_{12}O_{40}$ were observed at 2θ, degree (lattice plane) = 7.1 (001), 8.0 (110), 8.9 (011), 9.2 (101) and 18.4 (202). The diffraction peak and lattice plane were similar to that reported in the literature [31] and [JCPDF 43-0317].

The XRD patterns of $Na_2H[PM_{12}O_{40}]$ (M = Mo or W) compared to that of $H_3PM_{12}O_{40}$ (M = Mo or W) are presented in Figures 4.3 and 4.4.

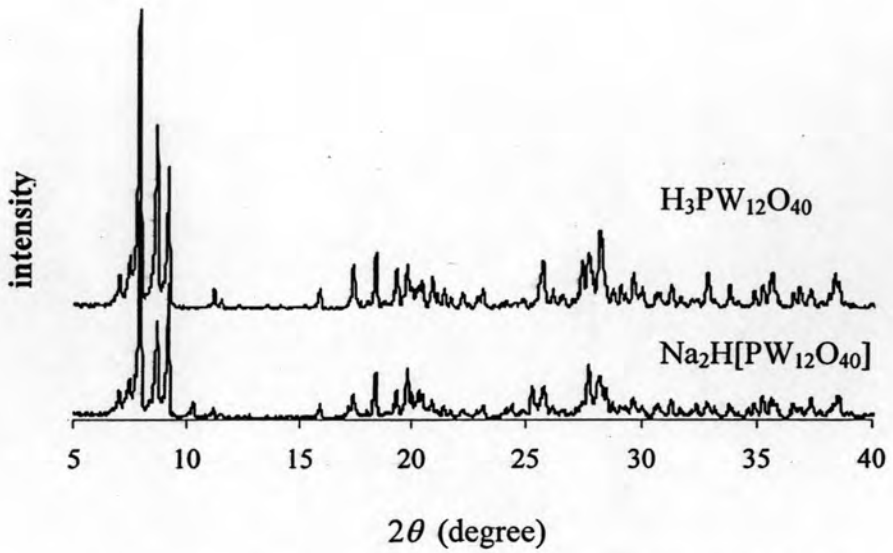

Figure 4.3 XRD patterns of $Na_2H[PW_{12}O_{40}]$ and $H_3PW_{12}O_{40}$.

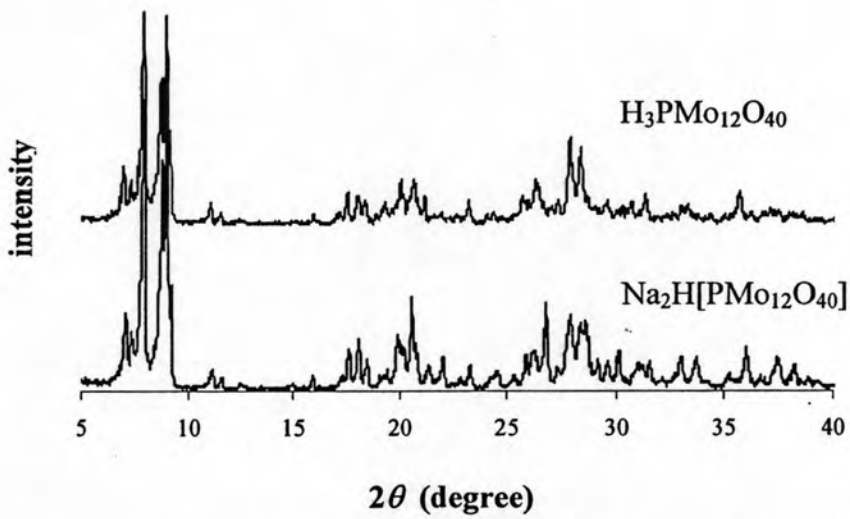

Figure 4.4 XRD patterns of $Na_2H[PMo_{12}O_{40}]$ and $H_3PMo_{12}O_{40}$.

From Figure 4.3 and 4.4, the XRD patterns of sodium acidic salt and the acid form are not different. Therefore, in order to confirm the presence of Na in the catalyst, the sample was analyzed by AAS technique. The results of %Na (by weight of catalyt) in $Na_2H[PMo_{12}O_{40}]$ and $Na_2H[PW_{12}O_{40}]$ are shown in Table 4.1.

Table 4.1 % Na in the sodium acidic salts

Entry	Catalyst	% Na	
		Calculated	Found
1	$Na_2H[PW_{12}O_{40}]$	1.91	1.86
2	$Na_2H[PMo_{12}O_{40}]$	2.96	2.86

The chemical formula of the catalyst was confirmed by %Na analysis which shows 1.86%Na in $Na_2H[PW_{12}O_{40}]$ and 2.86%Na in $Na_2H[PMo_{12}O_{40}]$ which is quite close to the calculated values.

The XRD patterns of vanadyl acidic salts: $(VO)H[PMo_{12}O_{40}]$ and $(VO)H[PW_{12}O_{40}]$ are presented in Figure 4.5.

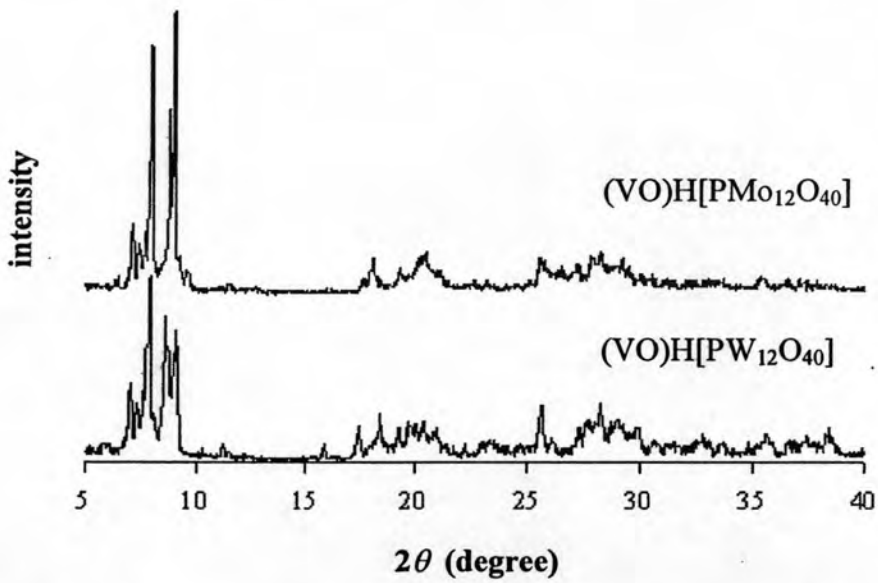

Figure 4.5 XRD patterns of vanadyl acidic salts: $(VO)H[PM_{12}O_{40}]$, (M = W or Mo)

The XRD diffraction peaks of $(VO)H[PMo_{12}O_{40}]$ and $(VO)H[PW_{12}O_{40}]$, were observed at 2θ, degree (lattice plane) = 7.1 (001), 8.0 (110), 8.9 (011), 9.2 (101) and 18.4 (202) and $(VO)H[PW_{12}O_{40}]$ shows 2θ, degree (lattice plane) = 7.1 (001), 8.0 (110), 8.8 (011), 9.2 (101) and 18.5 (202). In order to confirm the presence of

%V (by weight of catalyst) in the material, the sample was analyzed by ICP technique and the results are shown in Table 4.2.

Table 4.2 %V in the vanadyl acidic salts

Entry	Catalyst	%V	
		Calculated	Found
1	$(VO)H[PW_{12}O_{40}]$	1.72	1.63
2	$(VO)H[PMo_{12}O_{40}]$	2.69	2.71

%V in the $(VO)H[PW_{12}O_{40}]$ and $(VO)H[PMo_{12}O_{40}]$ show 1.63%V in $(VO)H[PW_{12}O_{40}]$ and 2.71%V in $(VO)H[PMo_{12}O_{40}]$ which is quite close to the calculated values.

The XRD patterns of the tetrabutylammonium salts of tungsto vanadophosphate: $(n\text{-}Bu_4N)_{3+x}[PW_{12-x}V_xO_{40}]$, (x = 1, 2 and 3) are shown in Figure 4.6.

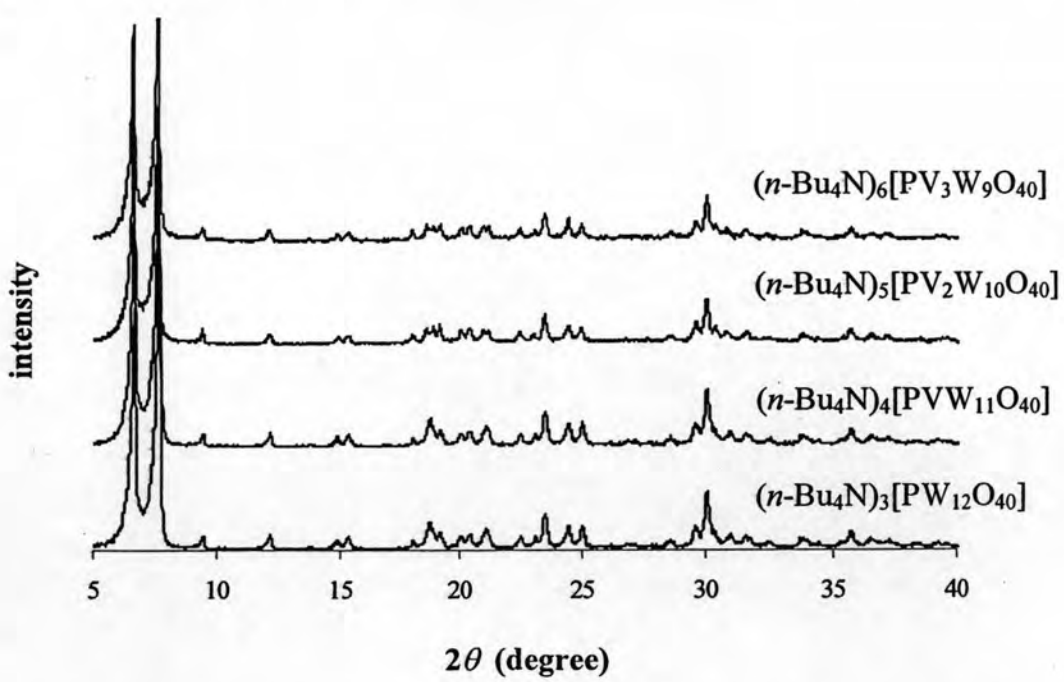

Figure 4.6 XRD patterns of tetrabutylammonium salts of tungsto vanadophosphate: $(n\text{-}Bu_4N)_{3+x}[PW_{12-x}V_xO_{40}]$, (x = 0, 1, 2 and 3)

The XRD patterns of the tetrabutylammonium salts of tungsto vanadophosphate: $(n\text{-}Bu_4N)_{3+x}[PW_{12-x}V_xO_{40}]$, (x = 0, 1, 2 and 3) show similar diffraction peaks at 2θ, degree (lattice plane) = 6.6 (002), 7.6 (200), 12.1 (111), 23.5 (401) and 30.0 (601). The XRD pattern was in good agreement with those reported in the literature [23, 32], 2θ = 6.6 (002), 7.6 (200), 12.1 (111), 23.5 (401), 30.0 (601).

In order to confirm the composition of the catalysts, the V content in the catalysts were determined by ICP analysis and are summarized in Table 4.3. The measured %V in the catalysts is in good agreement with the calculated values, indicating the successful formation of the catalysts.

Table 4.3 %V in the tetrabutylammonium salts of tungsto vanadophosphate: $(n\text{-}Bu_4N)_{3+x}[PW_{12-x}V_xO_{40}]$, (x = 1, 2 and 3)

Entry	Catalyst	% V	
		Calculated	Found
1	$(n\text{-}Bu_4N)_4[PVW_{11}O_{40}]$	1.37	1.29
2	$(n\text{-}Bu_4N)_5[PV_2W_{10}O_{40}]$	2.84	2.76
3	$(n\text{-}Bu_4N)_6[PV_3W_9O_{40}]$	3.88	3.75

4.2.2 Functional group of catalysts

The functional groups of catalysts were characterized by Fourier-transform infrared spectra (FT-IR). The structure of the Keggin polyoxometalate are shown in Figure 4.7.

(a)

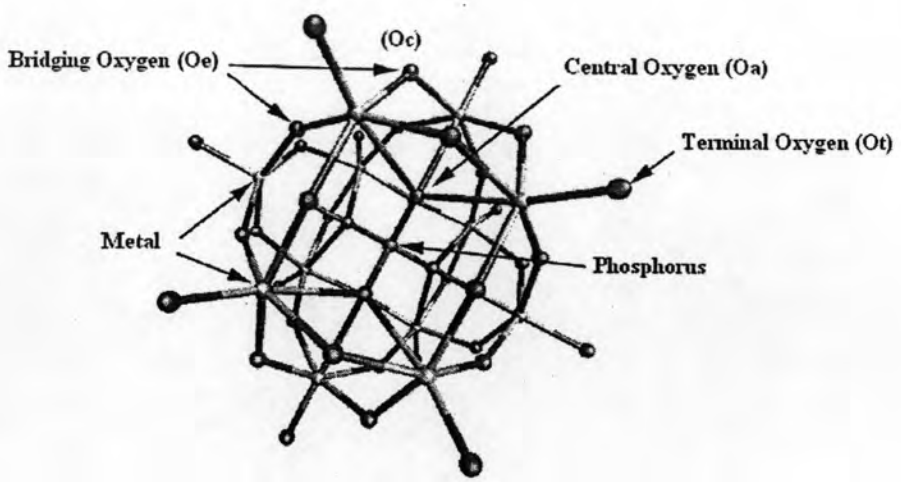

(b)

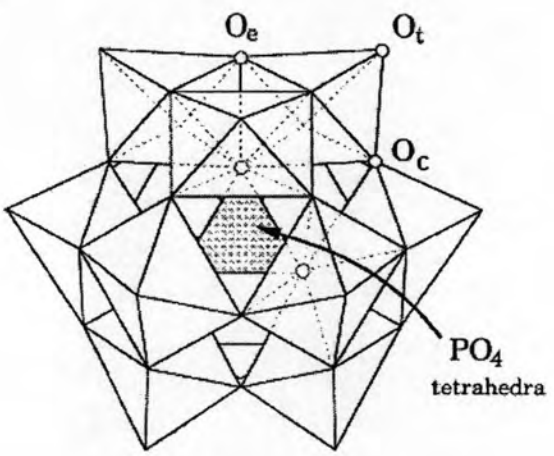

Figure 4.7 The structure of the Keggin polyoxometalate: (a) and (b) [33, 34].

The subscripted indicate oxygen bridging metal and the phosphorus heteroatom, O_a is the tetrahedral-coordinated phosphorous atom in the center of the structure, O_c is the corner-sharing bridging oxygen atoms, O_e is the edge-sharing bridging oxygen atoms and terminal oxygen atoms is O_t

All polyoxometalate catalysts were characterized by FT-IR. The FT-IR spectra of $H_3PM_{12}O_{40}$, $Na_2[HPM_{12}O_{40}]$ and $(VO)H[PM_{12}O_{40}]$: (M = W or Mo) are shown in Figure 4.8 and the results are summarized in Table 4.6.

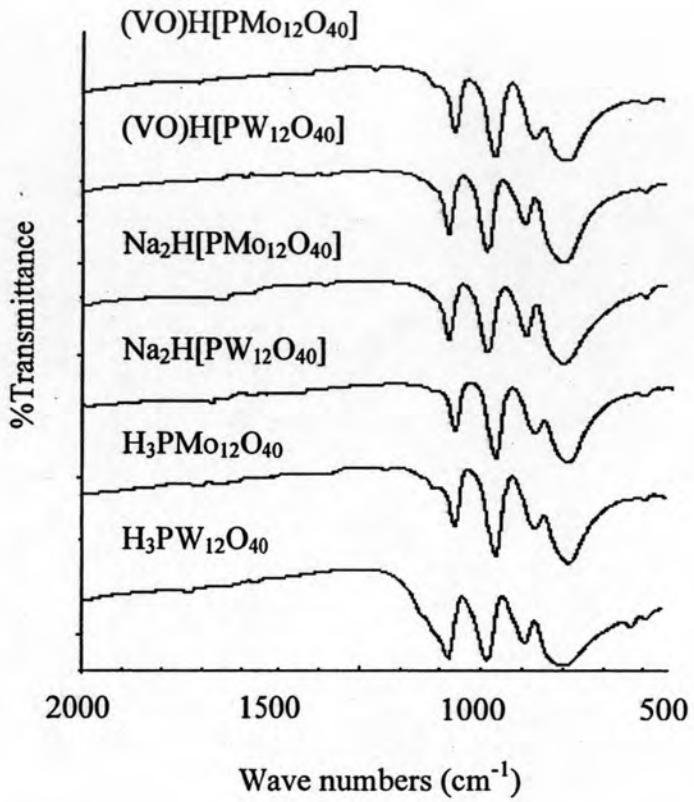

Figure 4.8 FT-IR spectra of $H_3PM_{12}O_{40}$, $Na_2H[PM_{12}O_{40}]$ and $(VO)H[PM_{12}O_{40}]$, (M = W or Mo).

Table 4.4 The vibration frequencies (cm^{-1}) of $H_3[PM_{12}O_{40}]$, $Na_2H[PM_{12}O_{40}]$ and $(VO)H[PM_{12}O_{40}]$, (M = W or Mo).

Catalysts	IR Wave numbers (cm^{-1})			
	M-O_e-M	M-O_c-M	M=O_t	P-O_a
$H_3PW_{12}O_{40}$	805	890	988	1080
$H_3PMo_{12}O_{40}$	788	867	964	1064
$Na_2H[PW_{12}O_{40}]$	789	889	983	1077
$Na_2H[PMo_{12}O_{40}]$	787	860	960	1063
$(VO)H[PW_{12}O_{40}]$	808	886	982	1080
$(VO)H[PMo_{12}O_{40}]$	791	867	960	1064

From Table 4.4, the FT-IR spectra of Keggin polyoxometalate catalysts show four characteristic bands (four types of oxygen atoms in the Keggin unit). For the first peak at 791-808 cm^{-1}, it is resulted from the ν_{as} (M- O_e- M) vibration mode, the second peak at 860-890 cm^{-1} is from the ν_{as} (M- O_c- M) vibration mode. The third peak at 960- 988 cm^{-1} comes from the ν_{as} (M- O_t) vibration mode while the fourth peak at 1063-1080 cm^{-1} is due to the ν_{as} (P- O_a) vibration mode [30, 35].

$H_3PMo_{12}O_{40}$, $H_3PW_{12}O_{40}$, $Na_2H[PMo_{12}O_{40}]$ and $Na_2H[PW_{12}O_{40}]$ show similar four bands to that reported in the literature [27, 29, 36]. The catalysts containing Mo have lower frequencies than the catalysts containing W. The vibration frequencies of catalysts are shown to depend on the nature of the cation. The FT-IR indicated all of the catalysts have framework of the Keggin structure.

The FT-IR spectra of tetrabutylammonium salts of tungstophosphate and tungsto vanadophosphate are shown in Figure 4.9 and the results are summarized in Table 4.5.

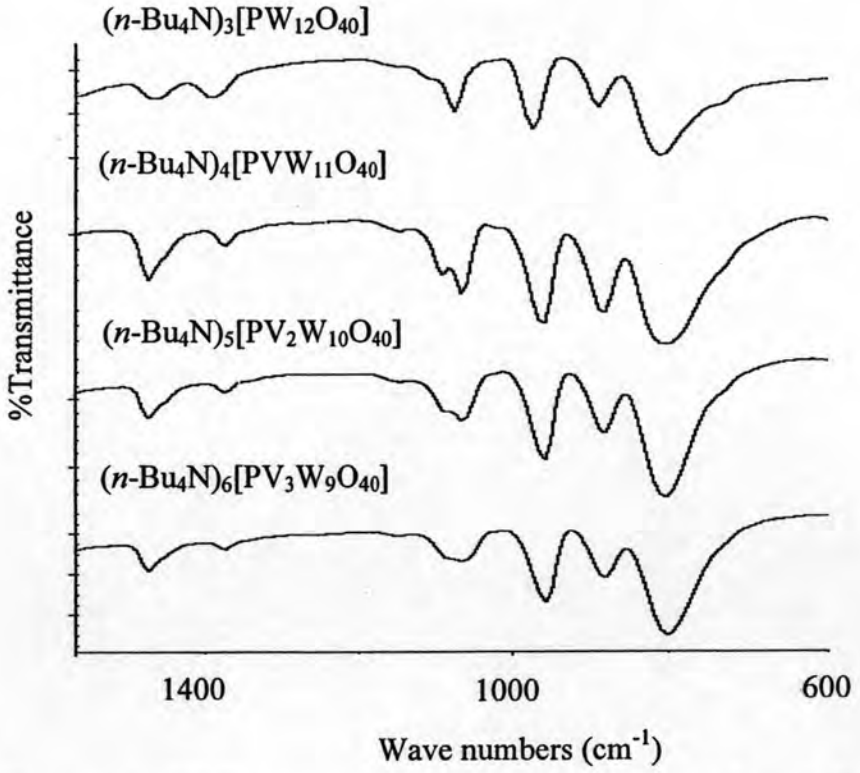

Figure 4.9 FT-IR spectra of $(n\text{-}Bu_4N)_{3+x}[PW_{12-x}V_xO_{40}]$ (x = 0, 1, 2 and 3).

Table 4.5 The vibration frequencies (cm^{-1}) of $(n\text{-}Bu_4N)_{3+x}[PW_{12-x}V_xO_{40}]$ (x = 0, 1, 2 and 3)

Catalysts	IR Wave numbers (cm^{-1})			
	M-O_e-M	M-O_c-M	M=O_t	P-O_a
$(n\text{-}Bu_4N)_3[PW_{12}O_{40}]$	813	895	978	1080
$(n\text{-}Bu_4N)_4[PVW_{11}O_{40}]$	809	886	965	1073, 1095
$(n\text{-}Bu_4N)_5[PV_2W_{10}O_{40}]$	808	886	962	1065, 1093
$(n\text{-}Bu_4N)_6[PV_3W_9O_{40}]$	808	882	960	1065, 1093

For tetrabutylammonium salts of tungstophosphate and tungsto vanadophosphate, the M-O_e-M and M-O_c-M bands appeared in the range of 808-813 cm^{-1} and 882-895 cm^{-1}, respectively. The bands at 960-978 cm^{-1} associated with the terminal M=O_t band. The P-O_a bands appeared in the range of 1065-1080 cm^{-1}. It occurs that this environment is distorted upon substitution with vanadium substituted in polyoxoanion and the vibration of polyoxoanion was changed, a shift of the frequencies to a lower wave number. This is in a good agreement with the literature [37, 38]. The splitting of the P-O bands into two components was also observed, this is due to the symmetry decrease of the PO_4 tetrahedral in the V-substituted complexes [39]. In addition, the peak at 1350-1500 cm^{-1} are assigned to the stretching vibration of the ammonium group in $(C_4H_9)_4N^+$, this result is similar to that reported [40]. The FT-IR indicated all of the catalysts have framework of the Keggin structure.

4.2.3 Absorption of metal in catalysts

The absorption of metal species in the catalyst was characterized by UV-Visible technique (UV-Vis). UV-Vis was recorded in the wavelength between 200 nm to 400 nm. All of polyoxometalate catalysts dissolved in acetonitrile was measured. The UV-Vis of catalysts are collected in Table 4.6.

Table 4.6 The absorption of metal in catalysts

Catalyst	Wavelength (nm) λ_{max}
$H_3PW_{12}O_{40}$	271
$H_3PMo_{12}O_{40}$	312
$Na_2H[PW_{12}O_{40}]$	270
$Na_2H[PMo_{12}O_{40}]$	310
$(VO)H[PW_{12}O_{40}]$	275
$(VO)H[PMo_{12}O_{40}]$	311
$(n\text{-}Bu_4N)_3[PW_{12}O_{40}]$	265
$(n\text{-}Bu_4N)_4[PVW_{11}O_{40}]$	261
$(n\text{-}Bu_4N)_5[PV_2W_{10}O_{40}]$	250
$(n\text{-}Bu_4N)_6[PV_3W_9O_{40}]$	245

From Table 4.6, it could be seen that the wavelength of the absorption maxima at about 245-312 nm. The absorption maxima of the Mo catalysts are higher than the W catalysts. This absorbance band is attributed to the charge-transfer bands of oxygen atom to metal center (ligand to metal charge transfer, LMCT). This represents the transfer of an electron from the Highest Occupied Molecular Orbital (HOMO) to the LUMO. Because the HOMO involves mostly the terminal oxygens, its energy is not greatly affected by changes in the HPA framework. However, the LUMO is greatly affected because it involves the bridging oxygens and the d-orbitals of the framework metals [41]. The wavelength of the absorption maxima of tetrabutylammonium as cation: $(n\text{-}Bu_4N)_{3+x}[PW_{12-x}V_xO_{40}]$ were at 265, 261, 250 and 245 nm, for x = 0, 1, 2 and 3, respectively. It was found that the wavelength (λ_{max}) of the absorption maxima of $(n\text{-}Bu_4N)_{3+x}[PW_{12-x}V_xO_{40}]$: (x = 0-3) shifted to shorter wavelength while the number of vanadium increased [30]. Substitution of V^{5+}ion, the energy and composition of the LUMO increases affect to the wavelength of the absorption maxima.

4.2.4 Reduction temperature of metal in catalysts

Temperature-programmed reduction (TPR) experiments were carried out in order to measure the reduction temperature of catalysts. In the TPR technique, the reduction of polyoxometalate by hydrogen occurs as follows: a hydrogen molecule is dissociated into hydrogen ion and electron. Hydrogen ion then reacts with oxygen of polyoxometalate to form a water molecule and then the metal is gain of electrons in which metal atoms have their oxidation number changed [26]. The lower reduction temperature corresponds to the higher reduction potential of the catalyst.

All of tetrabutylammonium salt as a cation: $(n\text{-}Bu_4N)_{3+x}[PW_{12-x}V_xO_{40}]$ (x = 0, 1, 2 and 3) showed the reduction peak within the temperature range 443-700 °C. The TPR profiles of catalysts are shown in Figure 4.10.

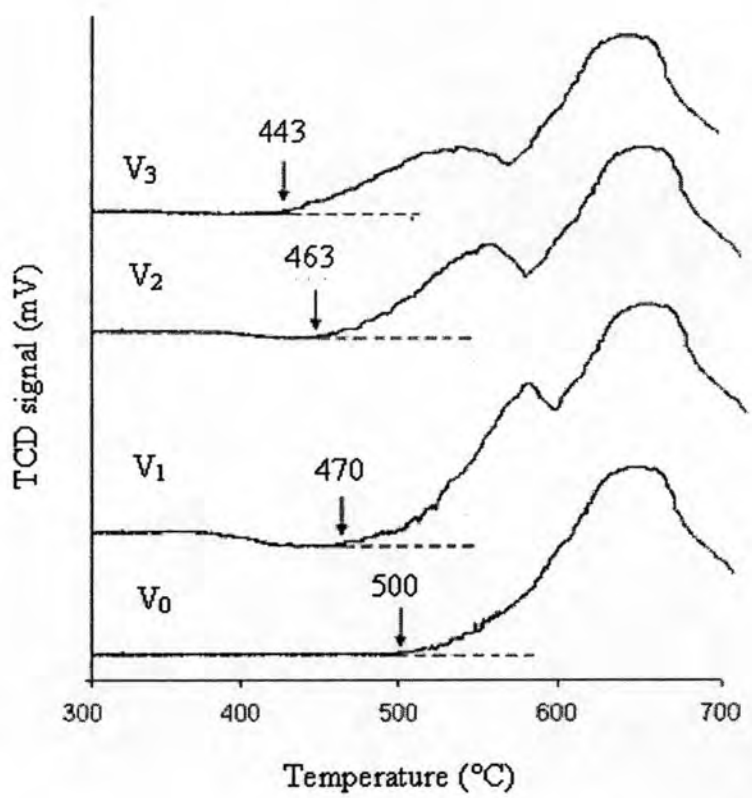

Figure 4.10 TPR profiles of $(n\text{-}Bu_4N)_{3+x}[PW_{12-x}V_xO_{40}]$ (x = 0, 1, 2 and 3).

Figure 4.11 compares the TPR profiles obtained from four catalysts. In V_0, only one broad reduction peak centered at 500-700 °C was recorded in TPR pattern. This has been reported to be attributed to the reduction of W^{6+} [42]. With the addition of V^{5+} in heteropolyanions, a small peak appeared in the temperature range of 443-600 °C. This was attributable to the reduction of V^{5+} [43]. The reduction temperature starts at 443, 463 and 470 °C for V_3, V_2 and V_1, respectively. Lower temperature of the reduction peaks indicates higher reduction potential of polyoxometalate and means that the catalyst is more active [44]. Therefore the order of reduction potentials is $V_3 > V_2 > V_1$.

4.3 Oxidation of model sulfur compounds

Benzothiophene (BT), dibenzothiophene (DBT) and 4,6-dimethyldibenzo-thiophene (4,6-DMDBT) were selected as representative of sulfur compounds present in diesel. Series of model reactions were carried out to optimize the reaction condition. Sulfone was the product from the oxidation reaction is shown in equations (4.1)-(4.3).

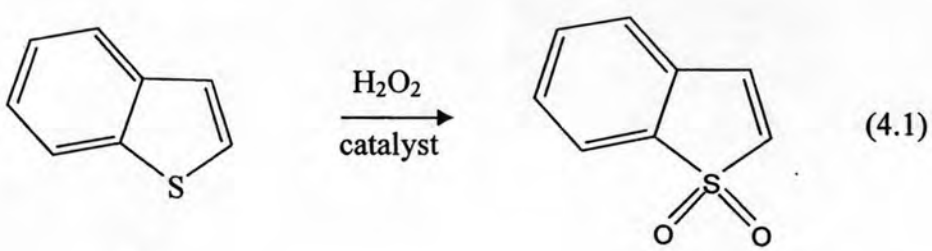

(4.1)

BT **BT Sulfone**

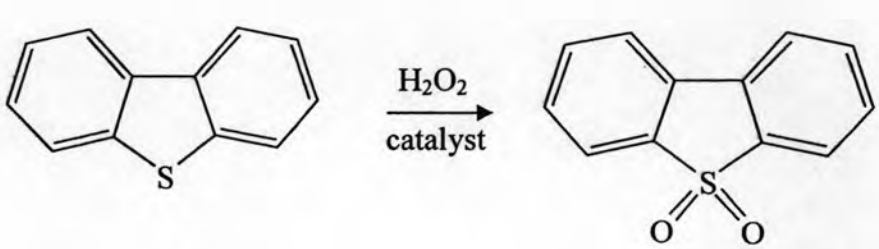

(4.2)

DBT **DBT Sulfone**

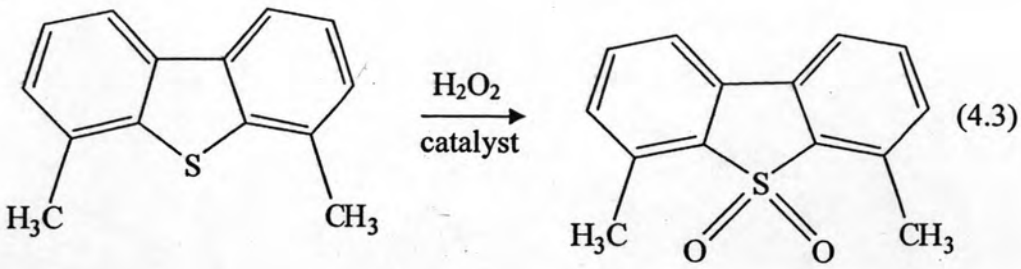

(4.3)

4,6-DMDBT **4,6-DMDBT Sulfone**

The products of oxidation of model sulfur compounds were analyzed by gas chromatography.

In case of synthesis of authentic 4,6-dimethyldibenzothiophene sulfone was synthesized and characterized by mass spectroscopy (MS).

4.4 Characterization of 4,6-dimethyldibenzothiophene sulfone

4.4.1 Molecular weight of 4,6-dimethyldibenzothiophene sulfone

Mass spectrometry is an analytical tool used for measuring the molecular weight of 4,6-dimethyldibenzothiophene sulfone. The mass spectrum is shown in Figure 4.11.

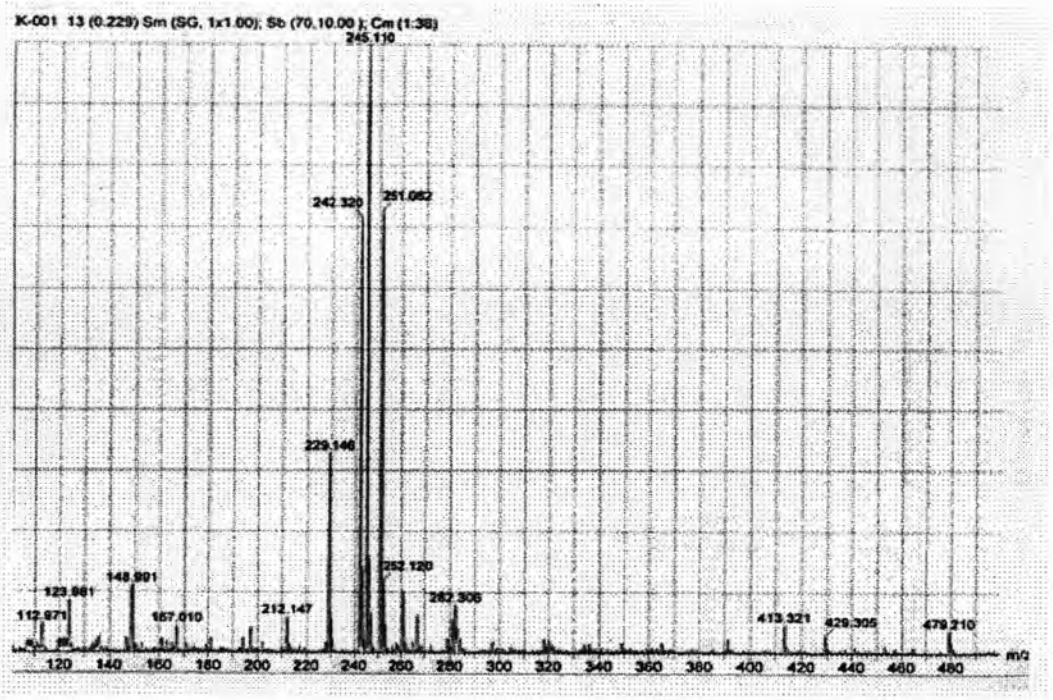

Figure 4.11 The mass spectrum of 4,6-dimethyldibenzothiophene sulfone.

The mass spectrum shows the Mw + H^+ = 245.1, Mw = 244.1. It is quite close to the molecular weight of 4,6-dimethyldibenzothiophene sulfone (Mw = 244.3).

4.5 The process of oxidative desulfurization

Generally, the oxidative desulfurization (ODS) process consists of two stages: the first step is an oxidation of organic sulfur-containing compounds, and the second step is the removal of oxidized sulfur-containing compounds by extraction.

The overall ODS reaction of the process is shown in Scheme 1, the sulfur compounds undergoes electrophilic addition of oxygen atoms from the hydrogen peroxide (H_2O_2) as an oxidizing agent to form the sulfones. The chemical and physical properties of sulfones are significantly different from substrate (model compound). Therefore, they can be easily removed by polar solvent extraction.

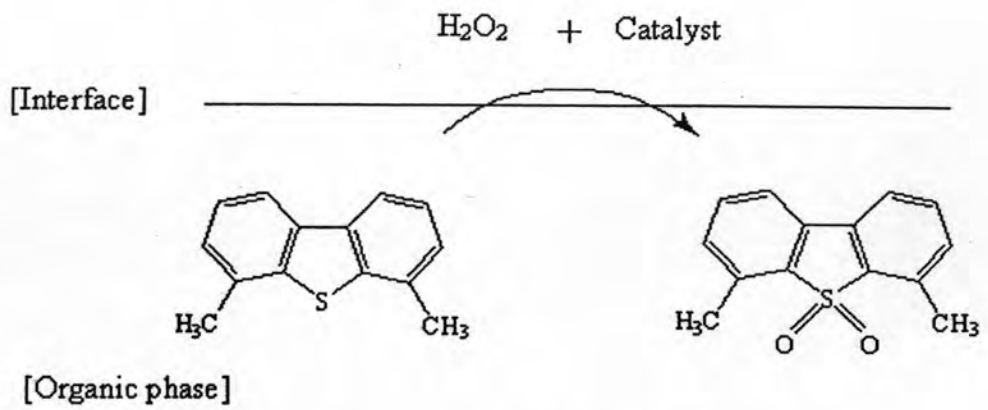

Scheme 1 Oxidation of model sulfur compound.

In this work, acetonitrile was chosen as solvent extraction. It was previously reported that the ability to extract sulfone corresponds to the polarity of solvent which decreased in order: acetonitrile > dimethyl formamide > ethanol [8]. Acetonitrile has a relatively low boiling point at 82 °C and can be easily separated by distillation from sulfones [45].

4.6 The solubility of catalysts

The solubility of various polyoxometalate catalysts in aqueous phase were checked. The results are collected in Table 4.7.

Table 4.7 Solubility of catalysts

Entry	Catalyst	AcOH + H_2O_2 (aqueous phase)
1	$H_3PW_{12}O_{40}$	Soluble
2	$H_3PMo_{12}O_{40}$	Soluble
3	$Na_2H[PW_{12}O_{40}]$	Soluble
4	$Na_2H[PMo_{12}O_{40}]$	Soluble
5	$(VO)H[PW_{12}O_{40}]$	Soluble
6	$(VO)H[PMo_{12}O_{40}]$	Soluble

Entry	Catalyst	AcOH + H_2O_2 (aqueous phase)
7	$(n\text{-}Bu_4N)_3[PW_{12}O_{40}]$	Insoluble
8	$(n\text{-}Bu_4N)_4[PVW_{11}O_{40}]$	Insoluble
9	$(n\text{-}Bu_4N)_5[PV_2W_{10}O_{40}]$	Insoluble
10	$(n\text{-}Bu_4N)_6[PV_3W_9O_{40}]$	Insoluble

From the results, the catalyst containing H, Na and VO as cation (entries 1-6) are found to be soluble in aqueous phase (AcOH and H_2O_2). On the contrary, the catalyst with tetrabutylammonium as cation (entries 7-10) are found to be insoluble in aqueous phase. Thus, the catalytic activity of tetabutylammonium as cation which the same heteropolyanion (entry 7) was lower than that of H, Na and VO (entries 1-6). It might be due to the solubility of catalyst in aqueous phase.

4.7 Oxidation of dibenzothiophene (DBT)

4.7.1 Oxidation of dibenzothiophene (DBT) with various catalysts

From our previous results on the effect of acetic acid addition on the oxidation of model sulfur compounds [23], the presence of acetic acid in the reaction could slightly promoted higher product yield (sulfone). The optimum amount of acetic acid determined from that work is [AcOH]/[H_2O_2] molar ratio = 1. Therefore, this ratio was used in this work.

Reaction between hydrogen peroxide and acetic acid results in the formation of peracetic acid, according to the equation (4.4).

$$CH_3COOH + H_2O_2 \longrightarrow CH_3CO_3H + H_2O \quad (4.4)$$

In this section, the catalytic activity of various synthesized catalysts were tested for the oxidation of model sulfur compounds. The reaction conditions used are similar to those reported in Komintarachat's work [23]: DBT 0.1 mmol, S/C molar ratio = 100, hexane (as a reaction solvent) 5 ml and acetonitrile (as a solvent extraction) 5 ml, [AcOH]/[H_2O_2] molar ratio = 1, temp. 60 °C and time 3 h. However, in this work two different O/S molar ratio = 5 and 10 were compared and the results are shown in Table 4.8.

Table 4.8 Oxidation of DBT with various catalysts

entry	catalyst	SulfoneYield (%)	
		O/S = 5	O/S = 10
1	$Na_2H[PW_{12}O_{40}]$	80	95
2	$Na_2H[PMo_{12}O_{40}]$	72	84
3	$H_3PW_{12}O_{40}$	80	93
4	$H_3PMo_{12}O_{40}$	70	82
5	$(VO)H[PW_{12}O_{40}]$	38	68
6	$(VO)H[PMo_{12}O_{40}]$	30	60
7	$(n\text{-}Bu_4N)_3[PW_{12}O_{40}]$	ND	52

Condition: DBT 0.1 mmol, S/C molar ratio = 100, hexane (as a reaction solvent) 5 mL and acetonitrile (as a solvent extraction) 5 mL and time 3 h. [AcOH]/[H_2O_2] molar ratio = 1, temp. 60 °C and time 3 h.
(S = Substrate, C = Catalyst, O = Oxidant)

ND = not determined

From table 4.8, when the oxidation was performed with various catalysts, at O/S molar ratio = 10, the sulfone yield (%) was increased with the increasing of H_2O_2 concentration in the reaction.

The oxidation reactivity order of the catalyst is: $Na_2H[PW_{12}O_{40}] \sim H_3PW_{12}O_{40} > Na_2H[PMo_{12}O_{40}] \sim H_3PMo_{12}O_{40} > (VO)H[PW_{12}O_{40}] > (VO)H[PMo_{12}O_{40}] > (n\text{-}Bu_4N)_3[PW_{12}O_{40}]$

Considering the comparative catalytic activity between the Mo- and W-containing catalysts, the experimental results showed that the catalytic activity of W containing catalyst for the oxidation of sulfur compounds is higher than the catalytic activity of Mo containing catalyst. As the $H_3PMo_{12}O_{40}$ have higher redox potential, this reveals that the activity is not governed by the catalyst's redox potential. It has been known that $H_3PW_{12}O_{40}$ and $H_3PMo_{12}O_{40}$ when reacted with H_2O_2 convert to polyoxoperoxo species, $[PM_{12}(O_2)O_{40}]^{3-}$ (M = W or Mo). The catalytic activities might be dictated by the oxidative activity of this derived polyoxoperoxo species [46]. It was reported in the literature that the $PW_{12}O_{40}^{3-}$ is much more effective for oxidation of cyclooctene than the $PMo_{12}O_{40}^{3-}$ [47].

Considering the type of cation in the catalyst, it can be seen that acid and sodium cations have comparable activity: $Na_2H[PW_{12}O_{40}] \sim H_3PW_{12}O_{40}$.

For the $(VO)^{2+}$ cation in the catalyst, it can be seen that the catalyst containing (VO)H cation has lower activity than that of $H_3PW_{12}O_{40}$. The catalytic acyivity of the $(VO)H[PM_{12}O_{40}]$ (M = Mo or W) in which vanadium is in V^{4+} bound to external oxygen atoms of the heteropolyanion is lower. It can also be seen that tetrabutylammonium salts show the lowest catalytic activity.

In conclusion, among various catalysts tested in this work, the experiment results show that the catalyst containing sodium acidic salt and acid with tungsten, $Na_2H[PW_{12}O_{40}]$ and $H_3PW_{12}O_{40}$ are the most active catalyst for the oxidation of model sulfur compound.

4.7.2 Effect of phase transfer catalyst (PTC)

From the previous report [48], PTC such as quaternary ammonium salts which facilitates the migration of catalyst from polar phase (aqueous phase) to apolar phase (organic phase). In this work, tetrabutylammonium bromide (n-Bu_4NBr) in the amount of PTC/catalyst molar ratio = 3 was used. The mechanism of oxidation reaction using PTC is shown in Scheme 2 and the results are shown in Table 4.9.

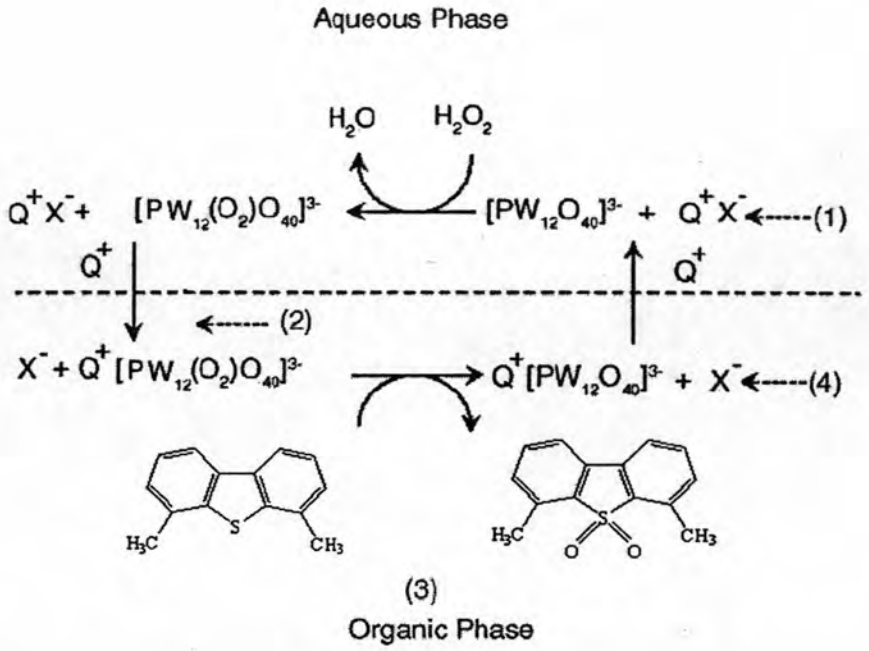

Scheme 2 Oxidation of model sulfur compounds when PTC was added [45].
Q^+X^- : tetrabutylammonium bromide

As suggested in many literatures [45, 49, 50], the oxidation of sulfur compounds with PTC may be depicted as a catalytic cycle, as seen in Scheme 2. It consists of four basic steps:

(1) In the presence of H_2O_2, $Na_2H[PW_{12}O_{40}]$ or $H_3PW_{12}O_{40}$, the metal precursor is oxidized and disaggregated to form peroxometal complex, $[PW_{12}(O_2)O_{40}]^{3-}$.

(2) Tetrabutylammonium salts with large lipophilic cation can function as phase transfer catalyst and transfer the peroxometal into organic phase.

(3) In organic phase, DBT are oxidized by peroxometal complex and gave rise to sulfone product.

(4) The reduced oxo species, which returns to aqueous phase and restores the catalytic cycle.

Table 4.9 The effect of phase transfer catalyst

catalyst	Phase transfer catalyst (PTC)	SulfoneYield (%)
$H_3PW_{12}O_{40}$	-	93
$H_3PW_{12}O_{40}$	*n*-Bu_4NBr	99
$Na_2H[PW_{12}O_{40}]$	-	95
$Na_2H[PW_{12}O_{40}]$	*n*-Bu_4NBr	100

Condition: DBT 0.1 mmol, S/C molar ratio = 100, O/S molar ratio = 10, hexane (as a reaction solvent) 5 mL and acetonitrile (as a solvent extraction) 5 mL, [AcOH]/[H_2O_2] molar ratio = 1, temp. 60 °C and time 3 h.

From the experimental data, adding of PTC gave higher sulfone yield, 100% for $Na_2H[PW_{12}O_{40}]$ and 99% for $H_3PW_{12}O_{40}$.

From the above experimental results (Table 4.11), the reaction with the phase transfer catalyst gave higher sulfone yield. Thus the next was to study the tetrabutylammonium salts as a cation.

4.7.3 Effect of vanadium (V) substitution

From the literature [51], it has been reported that the polyoxometalate with Keggin structure and their substituted species, in which one or more metal atoms have been replaced by V are highly efficient catalysts for oxidation of organic compounds. Also, in our previous report [23], the V catalyst with tetrabutylammonium cation gave higher sulfone yield. Thus, the tetrabutylammonium cation with different V substitution W in heteropolyanions was studied. The results are presented in Table 4.10.

Table 4.10 Oxidation of DBT using tetrabutylammonium cation containing vanadium (V)

entry	catalyst	SulfoneYield (%)
1	$(n\text{-}Bu_4N)_3[PW_{12}O_{40}]$	52
2	$(n\text{-}Bu_4N)_4[PVW_{11}O_{40}]$	72
3	$(n\text{-}Bu_4N)_5[PV_2W_{10}O_{40}]$	82
4	$(n\text{-}Bu_4N)_6[PV_3W_9O_{40}]$	95

Condition: DBT 0.1 mmol, S/C molar ratio = 100, O/S = 10, hexane (as reaction solvent) 5 mL and acetonitrile (as solvent extraction) 5 mL, $[AcOH]/[H_2O_2]$ molar ratio = 1, temp. 60 °C and time 3 h.

From Table 4.10, the substitution of V atom into $(n\text{-}Bu_4N)_{3+x}[PW_{12-x}V_xO_{40}]$ (x = 0, 1, 2 and 3) lead to obtain higher sulfone yield. The relative activity order is: $(n\text{-}Bu_4N)_6[PV_3W_9O_{40}]$ > $(n\text{-}Bu_4N)_5[PV_2W_{10}O_{40}]$ > $(n\text{-}Bu_4N)_4[PVW_{11}O_{40}]$ > $(n\text{-}Bu_4N)_3[PW_{12}O_{40}]$. This activity trend is in good relation with the trend of reduction temperature. Lower reduction temperature means that the catalyst was reduced more easily. The same trend in catalyst activity was reported on aerobic oxidation of tetrahydrothiophene using $H_{3+x}[PM_{12-x}V_xO_{40}]$ (M = Mo or W) catalysts, the catalytic activity order is $V_2 > V_1 > V_0$ [52].

The next step was to study and compare the reactivity of other refractory sulfur compounds (benzothiophene and 4,6-dimethyldibenzothiophene).

4.8 Oxidation of different model sulfur compounds: bezothiophene (BT) and dimethyldibenzothiophenes (DBTs)

To investigate the difference of reactivity of other sulfur compounds (4,6-DMDBT and BT) and compare to the DBT already studied. The same reaction condition as in section 4.7.2 was used. The results are collected in Table 4.11.

Table 4.11 Oxidation of different model sulfur compounds

Entry	catalyst	SulfoneYield (%)		
		DBT	4,6-DMDBT	BT
1	$Na_2H[PW_{12}O_{40}]$	95	60	36
2	$H_3PW_{12}O_{40}$	93	54	30
3	$(VO)H[PW_{12}O_{40}]$	68	35	22

Condition: substrate 0.1 mmol, S/C molar ratio = 100, O/S molar ratio = 10, hexane (as reaction solvent) 5 mL and acetonitrile (as solvent extraction) 5 mL, [AcOH]/[H_2O_2] molar ratio = 1, temp. 60 °C and time 3 h.

From the experimental, the effect of catalyst types are the same as previous section and the order of the catalyst activity is as follows: $Na_2H[PW_{12}O_{40}]$ ~ $H_3PW_{12}O_{40}$ > $(VO)H[PW_{12}O_{40}]$.

The results showed that the oxidative reactivity of the sulfur compounds decreased in the following order: DBT > 4,6-DMDBT > BT. The observed order of reactivity is different to that observed in the hydrodesulfurization process where the most sterically hindered 4,6-DMDBT is the least reactive. The same reactivity trend was reported in literature [7, 23]. The oxidation of model sulfur compounds (DBT, 4-MDBT, 4,6-DMDBT and BT) using *t*-BuOOH as an oxidant. The order of oxidation reactivity of these sulfur compound was found as follows: DBT > 4-MDBT > 4,6-DMDBT >> BT [8]. Also, it should be mentioned that the oxidation of model sulfur compound/H_2O_2/polyoxometalate, the oxidative reactivity decreased in the following order: DBT > 4,6-DMDBT > BT. For the formic acid/H_2O_2 system demonstrated completely different reactivity orders for the oxidation of DBTs, due to the important role of the molecular size of the catalyst. Formic acid-catalyzed reaction, the formic acid (small size) can interact with sulfur without any steric hindrance from alkyl groups. Therefore, the reactivity trend obtained in formic acid-catalyzed reactions reflects the intrinsic oxidation reactivities of DBTs: 4,6-DMDBT > DBT > BT [45].

In the oxidative desulfurization system, the effect of electron density on the sulfur atom and the steric hindrance of the methyl groups govern the reactivity. The higher reactivity of the DBT compared to BT is explained by the electron density on sulfur atom, the electron density on sulfur atom (5.758 for DBT and 5.739 for BT). Even though the electron density of 4,6-DMDBT is the highest (5.760), its reactivity is the lowest, this is due to the alkyl groups at 4 and 6 positions of 4,6-DMDBT that impose steric hindrance for the interaction of metal in catalyst with sulfur atom.

The electron density on sulfur atom was calculated by solving the Schrodinger equation [5]. The electron density on the sulfur compounds are shown in Figure 4.12.

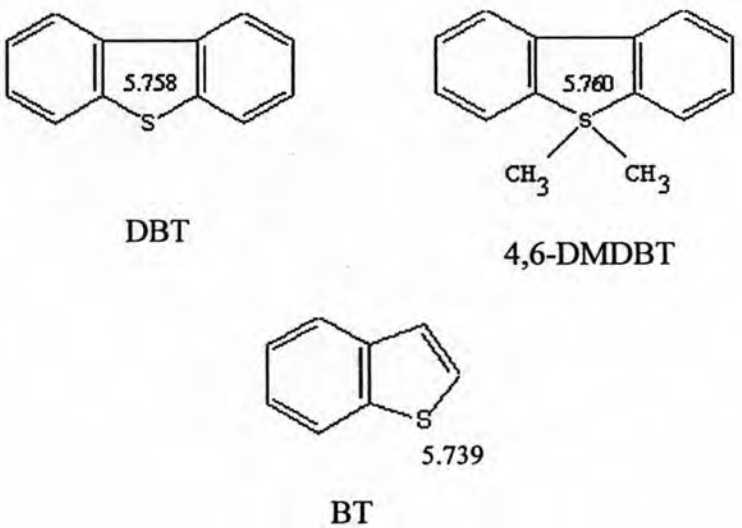

Figure 4.12 Electron density on sulfur compounds [5].

It was found that BT is the most difficult to be oxidized. In the next experiments, the amount of catalyst, reaction temperature and reaction time were increased to achieve higher %sulfone yield.

4.9 Oxidation of Benzothiophene (BT)

As BT is the most difficult to be oxidized, a more severe condition was attempted to increase %sulfone yield of BT. Using $Na_2H[PW_{12}O_{40}]$ as a catalyst at higher amount of catalyst (S/C molar ratio 50), higher temperature (70 °C) and longer

reaction time (5 h). The effect of oxidant amount on BT oxidation is investigated and the results are shown in Table 4.12.

Table 4.12 The effect of oxidant amount on benzothiophene oxidation using $Na_2H[PW_{12}O_{40}]$ as a catalyst

entry	O/S	SulfoneYield (%)
1	30	55
2	50	70
3	100	95

Condition: BT 0.1 mmol, S/C molar ratio = 50, hexane (as reaction solvent) 5 mL and acetonitrile (as solvent extraction) 5 mL, $[AcOH]/[H_2O_2]$ molar ratio = 1, temp. 70 °C and time 5 h.

From the result, %sulfone yield can be increased to 95% when using O/S molar ratio = 100. Thus, this condition is utilized for the next study on the oxidation of sulfur compounds in diesel fuel.

4.10 Study on the oxidation of sulfur compounds in diesel fuel

To investigate whether the oxidative desulfurization system in this work is effective for diesel fuel, the oxidative desulfurization of commercial diesel oil (containing 0.575 %wt of sulfur) was carried out. Acetonitrile was chosen as extractant solvent to remove oxidized sulfur compounds because the oil recovery was higher than DMF [5]. Alumina (Al_2O_3) was also used as adsorbent for further removal of the sulfone product. Sulfone product is more polar than the sulfur-containing compounds and is likely to bond strongly to an alumina adsorbent. %Sulfur removal in diesel fuel are shown in Table 4.13.

Table 4.13 % Sulfur removal in diesel fuel

Entry	Catalyst	Sulfur remained (wt%)	Sulfur removal (%)
1	$Na_2H[PW_{12}O_{40}]$	0.0810	86
2	$Na_2H[PW_{12}O_{40}]$+ n-Bu_4NBr	0.0056	99
3	$H_3PW_{12}O_{40}$	0.0912	85
4	$(n\text{-}Bu_4N)_6[PW_{12}O_{40}]$	0.1375	76
5	$(n\text{-}Bu_4N)_4[PVW_{11}O_{40}]$	0.0887	84
6	$(n\text{-}Bu_4N)_5[PV_2W_{10}O_{40}]$	0.0776	86
7	$(n\text{-}Bu_4N)_6[PV_3W_9O_{40}]$	0.0176	96

Recovery of oil 90%

Condition: diesel (0.5759 %wt sulfur) 10 ml, S/C molar ratio = 50, O/S molar ratio = 100, catalyst 0.036 mmol, acetonitrile 10 mL (as solvent extraction), [AcOH]/[H_2O_2] molar ratio = 1, Al_2O_3 as adsorbent, temp. 70 °C and time 5 h.

From the results obtained in this work, it was demonstrated that the trend of reactivity order of catalysts is the same as that obtained from the sulfur model compounds in the previous section (4.7.1 and 4.7.3). Sulfur reduction can be resulted in 5 h. In entry 2 when the phase transfer catalyst (PTC) was added to the $Na_2H[PW_{12}O_{40}]$ catalyst, %sulfur removal is up to 99% (from 0.575 %wt sulfur to 0.0056 %wt sulfur).

For comparison, it should be mentioned that from our previous result [23], the oxidation of diesel oil (0.5759 %wt sulfur) using $(n\text{-}Bu_4N)_4[V(VW_{11})O_{40}]$, in the presence of hydrogen peroxide/acetic acid at 70 °C in 5 h the removal of sulfur was 90%. The catalysts investigated in this work show higher activity. Another advantage is that shorter time is used compared to the time in the hydrogen peroxide/formic acid system (99% sulfur removal at 70 °C in 36 h) [5].

The Ministry of Energy of Thailand has limited the sulfur level in diesel fuel to 0.035 %wt sulfur [ASTM D4294]. The result obtained from this work is good, because the remaining sulfur in diesel oil was 0.0056% and 0.0176 %wt sulfur when

$Na_2H[PW_{12}O_{40}]$ mixed with phase transfer catalyst and $(n\text{-}Bu_4N)_6[PV_3W_9O_{40}]$ were used, respectively.

4.11 Proposed mechanism for the oxidation of sulfur compounds

The mechanism (in Scheme 3) can be described as follows:

The catalyst was reacted with oxidizing agent, peracetic acid (CH_3COOOH) which was formed from the reaction between hydrogen peroxide and acetic acid. The electrophilic intermediate (2) is formed after nucleophilic attact of peracetic acid (CH_3COOOH) on M^{n+}. Then (2) was transformed into M^{n+} peroxo species intermediate (3) and then (3) occurs on the homolytic cleavage to form $M^{(n-1)+}$ intermediate (4) and then (4) reacted with sulfur compound by forming O-S bond (5) and then the oxo species (1) reacted with peracetic acid, after that (4) reacted with sulfoxide and gave rise to sulfone (6), the only detected product.

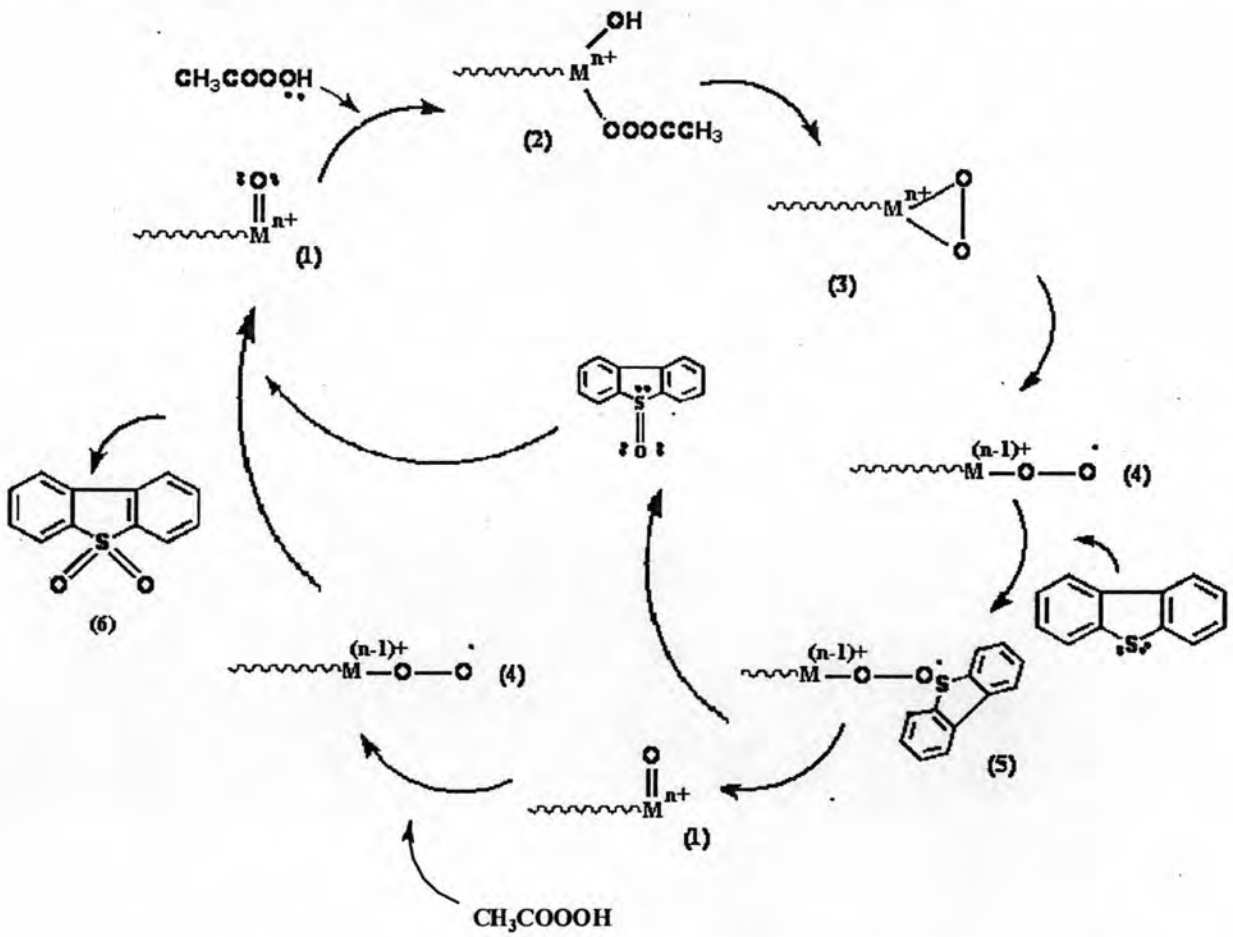

Scheme 3 Mechanism for the M-CH_3COOOH (M = V, W or Mo) catalyzed oxidation of sulfur compound [53, 54].